Int. J. Electrochem. Sci., 17 **(2022)** Article Number: 220511, doi: 10.20964/2022.05.01

International Journal of
ELECTROCHEMICAL
SCIENCE
www.electrochemsci.org

Short Communication

Study on the Corrosion of Steel Rebar Embedded in Engineered Cementitious Composites (ECCs) Containing Ceramic Waste by Electrochemical Methods

Lipeng Wu[1,2,3,*], *Zhengzheng Li*[2]

[1] State Key Laboratory of Building Safety and Built Environment, Beijing 100013, China
[2] School of Civil Engineering, Shijiazhuang Tiedao University, Shijiazhuang 050043, Hebei, China
[3] National Engineering Research Center of Building Technology, Beijing 100013, China
[*]E-mail: lipengwu@outlook.com

Received: 7 January 2022 / *Accepted:* 2 March 2022 / *Published:* 5 April 2022

The corrosion of steel rebar embedded in ECC materials containing ceramic waste was studied. Ground ceramic powder was used as an supplementary cementitious material that replaced cement by 30% to form a composite cementing system, and crushed waste ceramic was utilized as a fine aggregate that completely replaced the quartz sand commonly used in ECC preparation. Polyvinyl alcohol fiber was adopted as the reinforcing material. Electrical acceleration and dry-wet cycles were introduced to increase the corrosion rate. The corrosion potential was measured and EIS was performed using specimens at different stages of accelerated corrosion. By introducing an equivalent circuit model, the impedance spectroscopy data were explained quantitatively. The charge transfer resistance was used to measure the corrosion resistance of the steel bars embedded in the ECCs. The results show that through the use of ceramic waste, new ECCs with the same strength grade, elongation and corrosion resistance as conventional ECCs can be produced. The early anti-corrosion ability of the steel bar embedded in the new ECC first increases and then decreases with increasing fiber content, while the anti-corrosion ability in the later stages of corrosion is strengthened with increasing fiber content.

Keywords: ceramic waste; ECC; EIS; equivalent circuit; steel corrosion

1. INTRODUCTION

When deicing salt or marine chloride ions are present, rebar corrosion is the main durability problem faced by reinforced concrete structures. The corrosion of steel bars not only reduces the cross-sectional area of steel bars but also damages the bonding and anchoring between steel bars and concrete, thereby seriously weakening the structural integrity and safeness of these structures.

Engineered cementitious composites (ECCs) were proposed by Li in 1992 [1]. ECCs are strain-strengthening materials formed by adding randomly distributed short fibers to a brittle matrix [2]. ECCs do not contain coarse aggregate, which is widely used in ordinary concrete, and the typical particle size of the fine aggregates found in ECCs is approximately 0.1 mm. When the load is small, the composite material undergoes linear elastic deformation without cracks. As the load increases, the matrix cracks due to tension. Due to the bridging effect of the short fibers between cracks, the material forms multiple microcracks. The width of these cracks is less than 0.1 mm, and the spacing between them is approximately 10 mm. The "false strain" generated by multiple cracks greatly increases the macroscopic tensile strain of the material; the tensile strain hardening phenomenon occurs due to the fiber pulling out from the matrix, and the ultimate tensile strain can usually reach 3-5%. Because of the good mechanical properties and durability of ECCs, their application in the field of civil engineering has attracted widespread attention. At present, ECC materials have been used in bridge decks [3-5], prefabricated nonreinforced components [6, 7], nodes [8, 9], and structural repair and strengthening [10-12].

In the past ten years, many advances have been made in the improvement of ECC materials. To reduce the shrinkage of ECCs, Zhang et al. proposed a low-shrinkage ECC material (LSECC), and on this basis, a high-strength low-shrinkage ECC material was developed by introducing high-strength steel fibers [13]. The introduction of solid wastes to partially replace cement can not only increase the greenness of ECCs but also reduce costs, and it may also improve the workability, strength and durability of ECCs. In this regard, fly ash has become an important component of ECCs [14]. A class of self-levelling ECC was achieved using a large amount of fly ash, and the cement replacement rate reached up to 70% [14]. The replacement rate of cement by rice husk ash can also reach 30%, which can increase the tortuosity of the internal pore system and durability [15, 16]. The use of iron tailings powder can produce new ECCs with elongations of 2.3-3.3%, tensile strengths of 5.1-6.0 MPa, and compressive strengths of 46-57 MPa and reduce energy consumption by 10-32% and carbon emissions by 29-63% [17]. The use of wood-based cellulose nanocrystals can improve the compressive strength and the resistance to chloride ion intrusion of ECCs [18]. The introduction of ground granulated blast furnace slag can increase the strength of the matrix and the bridging ability of fibers, thereby increasing the ductility of the ECC material [19-21].

Ceramic waste is a solid waste that is produced worldwide. China is the world's largest producer and consumer of ceramic products. In recent years, the annual output of architectural ceramics has averaged 10 billion m^3 [22]. In general, ceramic production will generate waste levels of approximately 30% by weight [23]. In addition, the annual waste of demolished ceramics is also increasing. The sensible use of ceramic wastes can not only utilize the solid waste being rapidly produced but also reduce carbon emissions during ECC production. The alkalinity of the pore solution may be reduced due to the introduction of ceramic wastes, which leads to an unstable passive film formed on the surface of the steel bar. The ability to protect internal steel bars from corrosion is an important aspect of ECCs as suitable strengthening materials. This work studied the anti-corrosion properties of ECC materials with different fiber contents containing ceramic wastes.

2. EXPERIMENT

2.1 Materials and mix ratio

The cement used in the work was P.O.42.5 ordinary Portland cement (Hebei Zanhuang Jinyu Cement Co., Ltd.). Ground ceramic powder (demolished floor tiles, Gaoyi Lima Ceramics Co., Ltd.) was used as a supplemental cementitious material. Crushed ceramic tiles with a particle size of approximately 0.1 mm were put into a ball mill and ground with aluminum oxide grinding balls for two hours. Most of the particles of the obtained ground ceramic powder have a size of less than 50 microns, and the particle size distribution is close to that of ordinary Portland cement. The content of fine particles in the powder is slightly larger than that in ordinary Portland cement. Ceramic sand was made by crushing floor tiles, and its average particle size was between 0.075 mm and 0.15 mm. The appearances of the ground ceramic powder and crushed ceramic sand are shown in Figure 1. The particle size distributions of the cement and ceramic powder are shown in Figure 2, and the chemical compositions of the cement and ceramic powder are shown in Table 1.

Figure 1. Crushed ceramic sand(left) and ground ceramic powder(right) made from demolished floor tiles (Sand particle size: 0.075-0.15 mm; ground ceramic powder particle size: less than 60 μm).

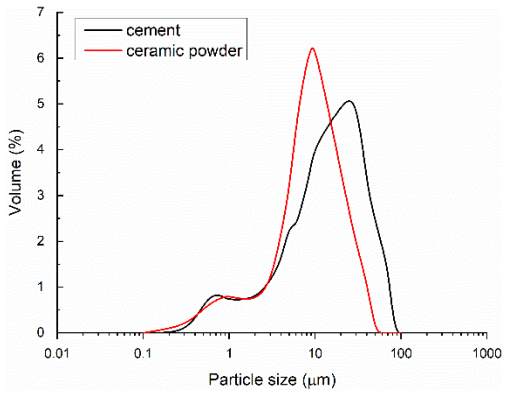

Figure 2. Comparison of the particle size distribution of cementitious materials. Note that ceramic powder is slightly finer than cement.

Table 1. Chemical compositions of raw materials (wt.%)

	SiO_2	Al_2O_3	CaO	Fe_2O_3	MgO	Na_2O	K_2O	SO_3	Cl
Ceramic powder	68.26	17.10	1.55	0.72	1.41	2.20	2.01	-	0.06
P.O.42.5	23.71	7.20	59.1	3.08	2.09	0.16	0.61	2.16	0.01

Table 1 shows that the content of CaO in the ground ceramic powder is less than 2%, which is far less than the content of CaO in the P.O.42.5 cement (usually approximately 60%). This may be an important reason behind the phenomenon that the ground ceramic powder cannot hydrate by itself when exposed to water. The contents of SiO_2 and Al_2O_3 in the ceramic powder are far greater than those of P.O.42.5 ordinary Portland cement.

The fiber used is PVA fiber, as shown in Figure 3, and its geometric and mechanical properties are shown in Table 2.

Figure 3. PVA fiber with a length of 8 mm and diameter of 40 μm.

Table 2. Properties of PVA fiber

Fiber type	Diameter (μm)	Length (mm)	Tensile strength (MPa)	Elongation (%)	Elastic modulus (GPa)	Density (kg/m^3)
PVA	40	8	1560	6.5	41	1300

The ECC mix ratios are shown in Table 3. In accordance with previous studies [24, 25], the replacement rate of cement by ceramic powder is set at 30%. All fine aggregates are made of crushed ceramic sand. In addition, P.O.42.5 ordinary Portland cement, class C fly ash, water, quartz sand with an average particle size of 0.075 mm-0.15 mm, and PVA fibers are used to prepare reference ordinary ECC materials. The matrix material ratio is 0.7 (cement): 0.3 (fly ash): 0.27 (water): 0.3 (quartz sand); the PVA fiber content is 1.6%. For the reference specimen, the 28 d compressive strength is 55.1 MPa, and the tensile strength is 4.41 MPa.

Table 3. Mix ratios of ECCs

Cement (kg)	Ceramic powder (kg)	Crushed ceramic sand (kg)	Water (kg)	PVA fiber (Vol %)	Compressive strength (MPa)	Tensile strength (MPa)
0.7	0.3	0.3	0.27	1.0%	56.3	1.97
0.7	0.3	0.3	0.27	1.2%	56.4	2.28
0.7	0.3	0.3	0.27	1.4%	56.2	2.72
0.7	0.3	0.3	0.27	1.6%	54.8	4.58
0.7	0.3	0.3	0.27	1.8%	54.7	4.62

The ultimate tensile strains of the ECC specimens obtained from the above mix ratios are all between 1.0% and 2.6%. Among them, the ultimate tensile strain of the ECC specimens with crushed ceramic sand is approximately 2.4%, which is very close to the ultimate tensile strain (2.6%) of the previously referenced ordinary ECC.

2.2 Specimen preparation

Hot rolled round bars (HPB 335, compliant with Chinese national standards GB/T 1499.1-2017) with a diameter of 16 mm were used. First, the steel bars were polished with a series of sandpaper with the finest size of P1000 (provided by 3M), then stains were removed with anhydrous alcohol, and finally the bars were rinsed with clean water and air-dried. After a copper wire was welded on one end, the steel bar was covered by epoxy resin, leaving only a length of 32 mm to be exposed to an accelerating corrosive environment. The rebar was centrally fixed in a mold with a diameter of 100 mm and a height of 100 mm. Cement, ceramic powder and ceramic sand were put into a mixer and stirred for two minutes, and then water and an appropriate amount of superplasticizer (depending on the fluidity of the slurry) were added. After stirring for another two minutes, PVA fibers were slowly added and the mixture was stirred for two more minutes. After the ECC was poured into the mold, it was vibrated and compacted and placed in a standard curing chamber for 28 d.

2.3 Test methods

2.3.1 Accelerated corrosion test

A conductive mesh woven from thin aluminum wires was wound on the surface of the ECC as the cathode, and steel rebar was used as the anode. The ECC specimen was placed into a NaCl solution with a concentration of 3.5%, and a direct current was applied to accelerate the corrosion rate. The direct current voltage was set to 16 V. The power was turned off after four hours, and the specimen was immersed in 3.5 wt.% NaCl solution for one hour to perform an open circuit potential test. For each cycle (one day), the specimens were immersed in the NaCl solution for five hours. Then, the ECC specimen was put into a vacuum container filled with saturated calcium hydroxide solution for

approximately two hours until the evolution of bubbles ceased. The specimen was removed from the solution, and the surface was dried for the electrochemical impedance spectroscopy test. After completion, the specimen was air-dried for approximately 17 hours as a cycle.

2.3.2 Electrochemical test

A three-electrode system was used to test the corrosion potential of the steel bars embedded in the ECC. The steel bar was the working electrode, the densely woven aluminum mesh was the auxiliary electrode, and a saturated calomel electrode was the reference electrode. A Zahner Zennium Pro electrochemical workstation and a two-electrode measurement system were used for the electrochemical impedance spectroscopy test. Tentative experiments showed that even if the ECC specimen was immersed in the electrolyte solution for five hours, there were still many "jumping points" in the electrochemical impedance spectroscopy test data. After immersion into a saturated calcium hydroxide solution under a continuous vacuum (pressure less than 0.2 atm) for one hour, the densely woven aluminum mesh was tightly wrapped on the ECC surface as an electrode of the two-electrode system. After removing samples from the NaCl solution, the surface was rapidly wiped with blotting paper, and then the electrochemical impedance spectroscopy test was performed immediately. For each frequency, 20 replicate tests were performed. After taking these measures, the tested impedance data were stable and smooth. During the electrochemical impedance spectroscopy test, the applied AC voltage amplitude was 10 mV, the frequency range was 10 mHz-100 kHz, and 10 test points were collected for each order of magnitude.

3. RESULTS AND DISCUSSION

3.1 Corrosion potential

The open circuit potential is shown in Figure 4. After the accelerated corrosion test started, the open circuit potentials of the steel bars embedded in each ECC specimen with different fiber contents were between -150 mV and -100 mV (vs. SCE), and there was no obvious correlation between the fiber content and the open circuit potential. Before 150 hours of accelerated corrosion, the open circuit potentials were not significantly reduced. Subsequently, the steel bars embedded in the ECCs had entered a stage of high corrosion probability. The steel bars embedded in the two specimens with lower fiber contents (1.0% and 1.2%) began to corrode first. As the fiber content increases, the time interval required for each steel bar to enter the corrosion stage generally increases. The steel bars embedded in the two specimens with high fiber contents (1.6% and 1.8%) finally began to rust. After 216 hours, all the steel bars entered the corrosion stage. After corrosion occurred, the open circuit potential continued to decrease, but they were all higher than -550 mV (vs. SCE).

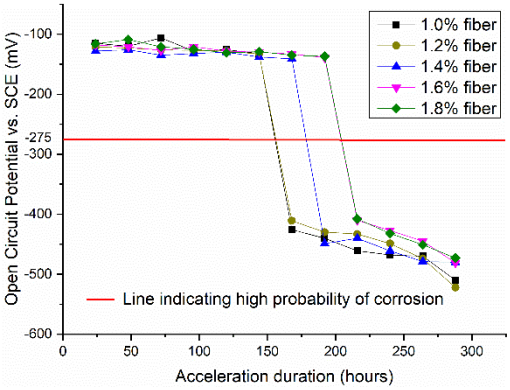

Figure 4. Open circuit potential vs. time of steel rebars embeded in ECCs with different fiber content in 3.5 wt.% NaCl (temperature: 22°C).

3.2 Electrochemical impedance spectroscopy

For each of the selected fiber contents, three time points were selected for electrochemical impedance spectroscopy. The three time points were 4 d, 10 d, and 12 d, corresponding to stages before corrosion, after corrosion begins, and during corrosion. During these tests, no visible cracks appeared on the ECC surfaces. Nyquist plots of the ECC specimens with various fiber contents at different stages of accelerated corrosion are shown in Figure 5.

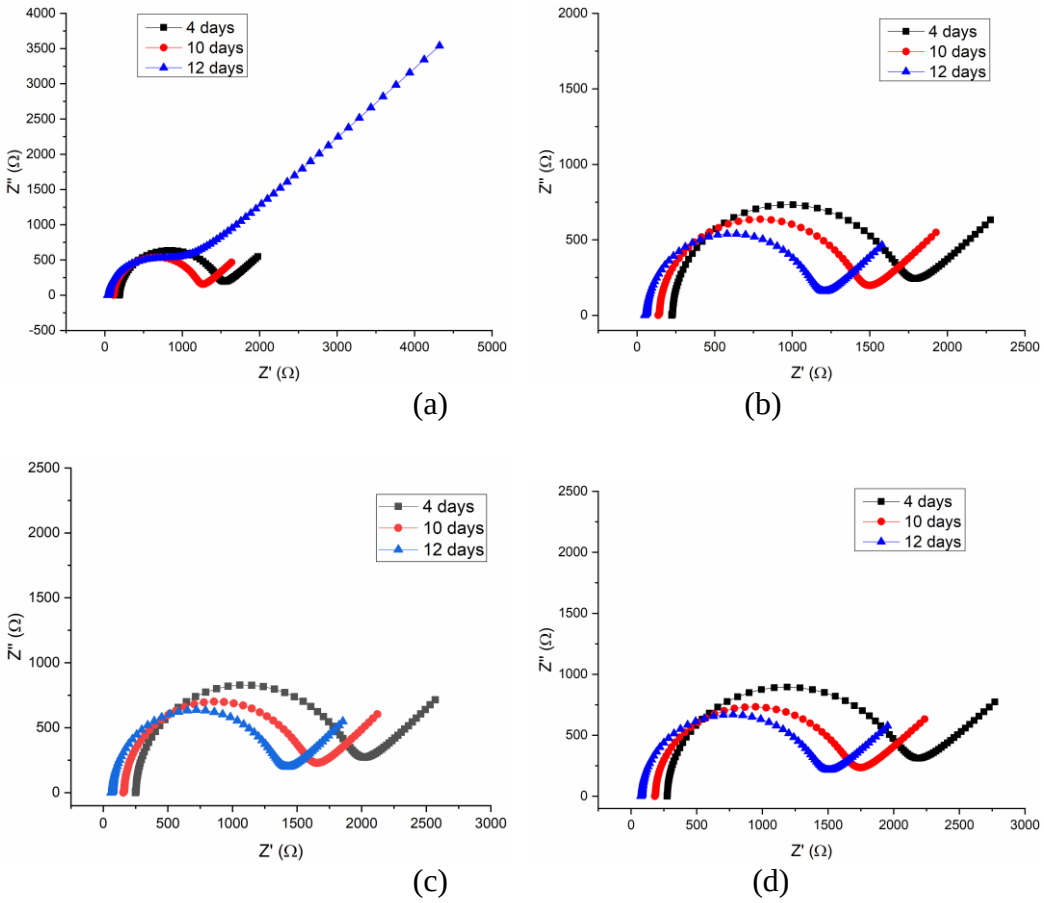

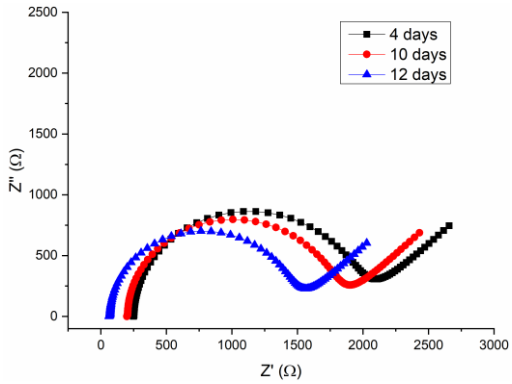

(e)

Figure 5. Nyquist plots of ECCs with different fiber contents at different immersion times. Fiber content: (a) 1.0%, (b) 1.2%, (c) 1.4%, (d) 1.6% and (e) 1.8%. (Corrosive medium: 3.5 wt. % NaCl solution; AC voltage: 10mV; frequency range: 10 mHz-100 kHz; temperature: 22°C).

To interpret the measured electrochemical impedance spectroscopy data, the equivalent circuit shown in Figure 6 was used. R_s represents the resistance of the concrete pore solution; when the passivation film was intact, C_f and R_f represent the capacitance and resistance of the passivation film (oxide film, a double-layer semiconductor), respectively. After the passivation film is broken, corrosion occurs. C_f and R_f represent the capacitance and resistance of the rust layer formed on the surface of the steel bar, respectively. The surface of the steel bar and the surrounding solution form a Helmholtz electric double layer, and its capacitance is represented by C_d. R_{ct} is the charge transfer resistance of the corrosion reaction, and W is the diffusion resistance. The Zahner Analysis software package was used to perform equivalent circuit fitting. The fitted values of each electronic component are shown in Table 4.

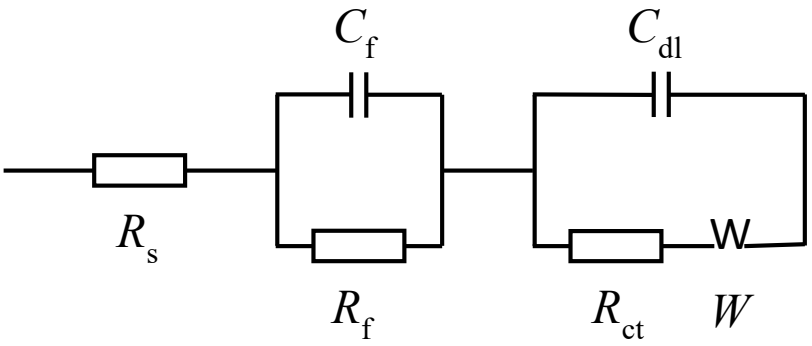

Figure 6. Equivalent circuit used to fit the EIS data. R_s is the solution resistance, and C_f and R_f correspond to the film capacitance and the film resistance, respectively. C_{dl} and R_{ct} represent the double layer capacitance and the charge transfer resistance, respectively. W is the Warburg diffusion element.

Table 4. Electrochemical parameters evaluated by fitting the impedance spectra after different durations of accelerated corrosion.

	1.0% fiber			1.2% fiber			1.4% fiber			1.6% fiber			1.8% fiber		
	3 d	10 d	12 d	3 d	10 d	12 d	3 d	10 d	12 d	3 d	10 d	12 d	3 d	10 d	12 d
R_c ($\Omega \cdot m^2$)	0.30	0.14	0.06	0.36	0.16	0.08	0.40	0.19	0.10	0.44	0.22	0.12	0.40	0.21	0.09
R_f ($m\Omega \cdot m^2$)	12	16	28	10	14	22	9	12	17	6	10	14	8	9	12
C_f ($mF \cdot m^{-2}$)	12	8	6	14	8	7	16	9	7	20	11	9	18	13	11
C_d ($mF \cdot m^{-2}$)	20	20	22	22	21	21	19	22	21	21	20	22	23	19	22
R_{ct} ($\Omega \cdot m^2$)	2.0	1.3	1.7	2.3	1.7	2.0	2.6	2.0	2.2	2.8	2.1	2.3	2.7	2.2	2.5
Y_0($S \cdot m^{-2} \cdot s$)	3.2	3.8	5.0	2.8	3.2	3.8	2.5	3.0	3.2	2.3	2.8	3.0	2.4	2.6	2.9

Note: The above data are normalized by the electrode area, which is 16.085 cm^2.

As reported by Chen et al. [26], fly ash is the most common and important supplementary cementitious material used in traditional ECCs, and quartz sand is the most commonly used fine aggregate. Ordinary Portland cement, fly ash, quartz sand, etc. were used to prepare ECCs [26]. Each cycle consists of a 24 h accelerated corrosion period (15 V) followed by a 24 h free standing period (0 V). The results showed that after 233 h and 257 h of accelerated corrosion, the charge transfer resistances were 13.7 $k\Omega \cdot cm^2$ and 10.5 $k\Omega \cdot cm^2$, respectively. In this work, wet-dry cycles were introduced into the accelerated corrosion regime, which are more likely to induce corrosion than constant immersion in solution. Table 4 shows that after 240 h (10 d) and 288 h (12 d) of accelerated corrosion, the charge transfer resistances were 22 and 25 $k\Omega \cdot cm^2$, respectively. It seems that the steel bars embedded in the new ECCs corrode at a slower rate than those in traditional ECCs, and the new ECCs can protect the steel bars better. This may be due to the use of the finely ground ceramic powder and crushed ceramic sand. Recently, Li et al. [27] found that the electric flux of the hardened paste using finely ground ceramic powder was 68%, 37%, 24% and 19% of the electric flux of the pure cement hardened paste, with cement replacement rates of 5.7%, 11.3%, 17% and 22.3%, respectively. Kannan et al. [28] reported that replacing 30% of cement with ground ceramic powder can reduce the electrical flux by 90%. Therefore, the addition of finely ground ceramic powder can make the microstructure of a material denser. Hossian et al. [29] and Herath et al. [30] reported the use of fly ash to reduce electrical flux and found that the use of fly ash to replace 50% and 65% of cement can reduce the electrical flux by 88.6% and 92.7%, respectively. These results indicate that the addition of finely ground ceramic powder has a similar effect on increasing the resistance to chloride ion intrusion compared with fly ash. For ceramic sand, Siddique et al. [31] observed that the water absorption rate of ceramic sand is higher than that of ordinary river sand, which can make the interfacial transition zone more compact, thereby reducing porosity. Higashiyama et al. [32] further noted that the use of ceramic sand can reduce the content of 0.05-2 micron pores in mortar from 0.0172 ml/g to 0.0125 ml/g, so the use of ceramic sand can significantly reduce the porosity. This explains that the use of finely ground ceramic powder and ceramic sand to prepare ECCs can not only improve the anti-chloride ion

intrusion abilities of the ECCs, thereby improving the anti-corrosion abilities of the embedded steel bars, but also form a new green and low-carbon ECC material.

Although the main purpose of adding fiber is to prevent cracking, the permeability of uncracked ECC is also important for the study of steel corrosion. The connected pores in the material create paths for the intrusion of harmful substances. Considering that the pore solution of ECCs is basically a saturated calcium hydroxide solution (its conductivity is approximately constant), it is a common practice to use pore solution resistance to characterize the connected porosity of a material.

Table 4 shows that at each time point of the test, the resistance of the ECC pore solution first increases and then decreases with increasing fiber content and reaches the peak value when the fiber content is 1.6%. This can be attributed to the fact that an appropriate amount of PVA fiber can form a good bond with the ECC matrix, and the bridging effect of the fibers can inhibit the appearance of microscopic shrinkage cracks in the ECC matrix. When the amount of fiber is too large, the resistance of the ECC pore solution decreases, indicating that the porosity of the ECC increases. This may be due to the increase in the volume of the interface zone between the fiber and the matrix. It is widely accepted that the porosity of the interfacial transition zone is much larger than that of the matrix.

As the accelerated corrosion process continues, the resistance of the ECC pore solution has a continuous decreasing trend. After 12 d of accelerated corrosion, the measured resistance drops to 20.0%, 22.2%, 25%, 27.3% and 22.5% of those of the 3 d value. If the conductivity of the pore solution is assumed to be constant during this period, the connected porosity of the ECC continues to increase, which means that the radial compression of the corrosion product causes circumferential tensile strain, which causes microdamage. The permeability of the ECC is proportional to the quadratic function of tensile strain [33], which makes it easier for substances, such as the oxygen required for corrosion, to intrude into the ECC matrix. It is worth noting that when the fiber content increases from 1.0% to 1.6%, the resistance change rate decreases sequentially; that is, the change rate of the connected porosity decreases sequentially. This may be attributed to the fact that as the fiber content increases, the bridging effect of the fibers gradually strengthens the inhibitory effect of the ECC matrix damage development. For example, when the fiber content is increased from 1.6% to 1.8%, the resistance change rate increases; that is, the change rate of the connected porosity increases. This may be because an excessively large fiber content is not conducive to the formation of a denser internal structure. This phenomenon is also observed in other fiber-reinforced cement-based materials [34].

The corrosion current density can be obtained from the linear polarization resistance R_{p} according to the Stern–Geary equation:

$$i_{\mathrm{corr}} = B/R_{\mathrm{P}} \tag{1}$$

Where

$$B = \frac{b_a b_c}{2.303(b_a + b_c)}$$

$$\mathrm{CR} = 304.2/R_{\mathrm{P}}\ (\mathrm{mm/yr}) \tag{2}$$

B is the so-called Stern–Geary constant (26 mV); b_a and b_c are the Tafel slopes of the anode and cathode reactions, respectively. Equation (2) can be derived from Faraday's law to calculate the corrosion rate (CR).

The polarization resistance R_p can be replaced by the charge transfer resistance R_{ct} obtained from the equivalent circuit fitting of electrochemical impedance spectroscopy data. Table 4 shows that before corrosion starts, the charge transfer resistance first increases and then decreases with increasing fiber content, and the charge transfer resistance reaches a peak value when the fiber content is 1.6%. As analyzed in the previous section, when the fiber content is not too large, the bridging effect of the fiber restricts the microscopic shrinkage and cracking of the ECC. This restriction is intensified with increasing fiber content. Since the propagation of microscopic cracks in the ECC matrix is restricted, it is more difficult for chloride ions to penetrate, and the passive film of the steel bar is less damaged. When the fiber content exceeds 1.6%, the harmful effect caused by the increase in the proportion of the interface zone between the fiber and the ECC matrix exceeds the beneficial effect of the fiber such that the chloride ion can migrate to the steel bar surface more easily to destroy the passive film of the steel bar.

After corrosion starts, especially after corrosion continues for a period of time, the charge transfer resistance tends to increase with increasing fiber content, which shows that, within the scope of this study, increasing the fiber content has a significant effect on reducing the reinforcement corrosion rates during the later stages of corrosion. This may be attributed to the elastic modulus of the PVA fiber being greater than that of the ECC matrix. The larger the fiber content is, the greater the overall tensile elastic modulus of the ECC. In this situation, a greater pressure on corrosion products will occur with the same circumferential strain. As the corrosion products continue to accumulate on the surface of the steel bars, the compression effect of the surrounding ECC makes the corrosion product layer gradually dense, which limits the transmission of external oxygen to the uncorroded steel bars and effectively inhibits the corrosion rate.

4. CONCLUSIONS

Using an appropriate amount of ground ceramic powder instead of cement and completely using crushed ceramic sand instead of quartz sand, a new type of ECC with mechanical properties similar to those of traditional ECC can be obtained.

A stable passive film can form on the steel bar surface in the new ECC.

With the increase in the PVA fiber content, the resistance of the connected pore solution of the new ECC first increases and then decreases, and there is an optimal content with regard to durability.

The continuous anti-corrosion ability of the new ECC using ceramic waste is enhanced with increasing PVA fiber content.

ACKNOWLEDGEMENTS

The authors gratefully acknowledge the financial support for this study from the Opening Funds of State Key Laboratory of Building Safety (BSBE2019-07) and Natural Science Foundation of Hebei Province (E2021210088)

References

1. V. C. Li, *J. Mater. Civ. Eng*., 4 (1992) 41.
2. V. C. Li, H. Stang, H. Krenchel, *Mater. Struct*., 26(1993) 486.
3. M. D. Lepech, V. C. Li, *Mater. Struct*., 42 (2009) 1185.
4. H. Ma, Z. G. Zhang, B. Ding, X. Tu, *Constr. Build. Mater*., 191 (2018) 679.
5. J. Zhao, C. Yan, S. Liu, J. Zhang, Y. Zhang, *Road Mater. Pavement Des*., (2021) 1.
6. L. H. Larusson, G. Fischer, J. Jonsson, *Eng. Struct*., 46 (2013) 104.
7. X. L. Li, Y. Li, M. Yan, W. N. Meng, X. Lu, K. Z. Chen, Y. Bao, *Eng. Struct*., 247 (2021) 113115.
8. S. H. Said, H. A. Razak, *Constr. Build. Mater*., 107 (2016) 226.
9. R. Zhang, K. Matsumoto, T. Hirata, Y. Ishizeki, J. Niwa, *Eng. Struct.*, 86 (2015) 146.
10. M. E. Gulsan, A. Mohammedameen, M. Sahmaran, A. Nis, R. Alzeebaree, A. Cevik, *Adv. Concr. Constr*., 6 (2018) 199.
11. H. Y. Qian, J. C. Guo, X. M. Yang, F. Lin, *Structures*, 34 (2021) 1212.
12. H. E. Yucel, H. Jashami, M. Sahmaran, M. Guler, M. Sahmaran, *Mag. Concr. Res.*, 65 (2013) 108.
13. Z. B. Wang, J. Zhang, J.H. Wang, Z. J. Shi, *J. Compos. Mater*., 49 (2015) 2169.
14. I. Abdulkadir, B. S. Mohammed, M. S. Liew, M. M. A. Wahab, *Case Stud. Constr. Mater*., 14 (2021) e00525.
15. F. B. P. da Costa, D. P. Righi, A. G. Graeff, L. C. P. da Silva, *Constr. Build. Mater.*, 213 (2019) 505.
16. Z. G. Zhang, F. Yang, J. C. Liu, S. P. Wang, *Cem. Concr. Res.*, 137 (2020) 106200.
17. X. Y. Huang, R. Ranade, V. C. Li, *J. Mater. Civ. Eng.*, 25 (2013) 923.
18. H. J. Lee, W. Kim, *Constr. Build. Mater.*, 238 (2020) 117754.
19. I. Lim, J. C. Chern, T. Liu, Y. W. Chan, *J. Mar. Sci. Technol.*, 20 (2012) 319.
20. Y. S. Liu, X. M. Zhou, C. B. Lv, Y. Z. Yang, T.A. Liu, *Adv. Civ. Eng.*, 2018 (2018) 7987589.
21. Q. Wang, M. H. Lai, J. Zhang, Z. B. Wang, J. C. M. Ho, *Constr. Build. Mater.*, 247 (2020) 118211.
22. X. T. Ma, T. Z. Zhang, X. Q. Shen, Y. J. Zhai, J. L. Hong, *J. Cleaner Prod*., 337 (2022) 130606.
23. M. Samadi, G. F. Huseien, H. Mohammadhosseini, H. S. Lee, N. H. A. S. Lim, M. M. Tahir, R. Alyousef, *J. Cleaner Prod.*, 266 (2020) 121825.
24. L. Li, W. F. Liu, Q. X. You, M. C. Chen, Q. Zeng, *J. Cleaner Prod.*, 259 (2020) 120853.
25. L. G. Li, Z. Y. Zhuo, J. Zhu, J. J. Chen, A. K. H. Kwan, *Powder Technol.*, 355 (2019) 119.
26. Z. Chen, G. Zhang, E. H. Yang, *Electrochim. Acta*, 261 (2018) 402.
27. L. G. Li, Z. Y. Zhuo, A. K. H. Kwan, T. S. Zhang, D. G. Lu, *Powder Technol.*, 367 (2020) 163.
28. D. M. Kannan, S. H. Aboubakr, A. S. El-Dieb, M. M. Reda Taha, *Constr. Build. Mater.*, 144 (2017) 35.
29. M. M. Hossain, M. R. Karim, M. Hasan, M. K. Hossain, M. F. M. Zain, *Constr. Build. Mater.*, 116 (2016) 128.
30. C. Herath, C. Gunasekara, D. W. Law, S. Setunge, *Constr. Build. Mater.*, 258 (2020) 120606.
31. S. Siddique, S. Shrivastava, S. Chaudhary, *Constr. Build. Mater.*, 173 (2018) 323.
32. H. Higashiyama, F. Yagishita, M. Sano, O. Takahashi, *Constr. Build. Mater.*, 26 (2012) 96.
33. H. Z. Liu, Q. Zhang, C. S. Gu, H. Z. Su, V. C. Li, *Cem. Concr. Compos.*, 72 (2016) 104-113.
34. F. Y. Liu, K. Xu, W. Q. Ding, Y. F. Qiao, L. B. Wang, *Cem. Concr. Compos.*, 123 (2021).